1 **Aerosol optical characteristics in the urban area of Rome, Italy, and their impact**

2 **on the UV index.**

4 Monica Campanelli[1], Henri Diémoz[2], Anna Maria Siani[3], Alcide di Sarra[4], Anna Maria Iannarelli[5], Rei

5 Kudo[6], Gabriele Fasano[3,2], Giampietro Casasanta[1], Luca Tofful[7], Marco Cacciani[3], Paolo Sanò[1],

6 Stefano Dietrich[1]

8 [1] Institute of Atmospheric Sciences and Climate, National Research Council, Rome, Italy

9 [2] Aosta Valley Regional Environmental Protection Agency (ARPA), Saint-Christophe, Italy

10 [3] Sapienza University of Rome, Department of Physics, Rome, Italy

11 [4] ENEA, Laboratory for Earth Observations and Analyses, Frascati, Italy

12 [5] SERCO, Italy

13 [6] Meteorological Research Institute, Japan Meteorological Agency, Tsukuba, 305-0052, Japan

14 [7] Institute of Atmospheric pollution, National Research Council, Italy

16 Corresponding to: m.campanelli@isac.cnr.it

18 **Abstract**

19 The impact of the aerosol optical properties on the ultraviolet index (UVI) in the urban area of Rome is

20 investigated in this study. In particular, the influence of aerosol optical depth (AOD) and single scattering

21 albedo (SSA), estimated at the wavelength of 340 nm, and of the Ångström exponent, calculated in the

22 range 340-500 nm, over a period of 11 years (2010-2020) in the months from March to September are

23 analyzed. The UVI is monitored by a Brewer spectrophotometer, whereas measurements of the direct

24 sun and diffuse sky irradiances are performed by a co-located PREDE-POM sun-sky radiometer of the

25 ESR/SKYNET network; the aerosol optical properties are obtained by the Skyrad MRIv2 retrieval. A

26 novel method, based on physical principles and easily adaptable to other contexts, is developed to

27 extrapolate the aerosol properties to the UV range during periods when only visible to near infrared

28 measurements are available. The retrievals from the sun-sky radiometer are consistent with the chemical

29 characterization of urban PM_{10} (particulate matter 10 micrometers or less in diameter) samples, collected

30 during an intensive field campaign held in summer 2011 in the same site (URBan Sustainability Related

31 to Observed and Monitored Aerosol – URBS ROMA). The PM macro-components identified during the

32 campaign are grouped in order to evaluate the contribution of the main macro-sources (SOIL, SEA,

33 SECONDARY INORGANIC, ORGANICS and TRAFFIC) whose relative role is indeed expected to

34   strongly affect the aerosol absorption capability. The surface forcing efficiency, calculated as the change

35   in the UV index for a unit AOD variation, shows that AOD is the primary parameter affecting the surface

36   irradiance under clear sky conditions in Rome. SSA and the Ångström exponent are also identified as

37   secondary influencing factors, i.e., the surface forcing efficiency is found to be greater for smaller zenith

38   angles and for larger and more absorbing particles in the UV range (such as, e.g., mineral dust).

39

1. Introduction

41   The aerosol influence on the incoming and outgoing solar radiation is a widely studied topic because of

42   its relation with the Earth's radiative balance and climate. Indeed, the aerosol capability of attenuating

43   the UV radiation is responsible for its short and long-term variations and it has important implications

44   for tropospheric photochemistry, human health, and for the properties of organic materials, such as

45   plastics and wood routinely exposed solar radiation as well as aquatic systems (Dickerson et al., 1997;

46   He and Carmichael, 1999; Castro et al., 2001; Casasanta et al., 2011; Mok et al. 2018). Nevertheless,

47   various aspects are still uncertain because the columnar absorbing and scattering properties of

48   suspended particles are not very common in this wavelength region.

49   The aerosol optical depth (AOD) and single scattering albedo (SSA), that is the ratio of the aerosol

50   scattering to extinction coefficient, representing an index of the aerosol absorption capability, are

51   important radiative parameters to determine the aerosol effect on the UV irradiance at the surface.

52   Reuder and Schwander (1999) demonstrated that more than 80% of the aerosol effect on surface UV

53   radiation due to increasing turbidity of the atmosphere can be estimated through aerosol optical depth

54   and single scattering albedo. Strong UV absorption by aerosol, characterized by low SSA values at

55   wavelengths shorter than 400 nm, is commonly attributed to organic aerosols that absorb predominantly

56   in the UV region (Martins et al., 2009) and trigger a stronger wavelength dependence than for the pure

57   black carbon component (Kirchstetter et al., 2004). In effect, an enhancement of aerosol absorption at

58   UV wavelengths was observed in urban cities such as Rome, Italy (Ialongo et al., 2010) and Athens,

59   Greece (Kazadzis et al., 2016), especially in winter. Also, mineral components show a significant

60   absorption in the UV region, as highlighted by Meloni et al. (2006). Di Sarra et al. (2002), Panicker et

61   al. (2009), and Antón et al. (2011), among others, have shown that an increase of AOD induces a

62   reduction of the UV index (UVI), a relevant quantity expressing the levels of UV radiation potentially

63   harmful to human health. These studies suggested that a unit increase in aerosol optical depth at about

64   400 nm may produce a significant decrease of UVI which depends on the solar zenith angle and aerosol

65   properties, and may exceed 50%. More recently, Fountoulakis et al. (2021) showed that the positive

66   trends in UV irradiance detected in Rome in specific months during the last decades are possibly driven

67   by changes in clouds and/or aerosols.

This work is aimed at determining, for the first time in Rome, the effect of aerosol optical properties on UV radiation, evaluating the role of SSA, AOD and Ångström exponent. Aerosol optical properties were provided by a PREDE-POM sun-sky radiometer of the ESR/SKYNET (www.euroskyrad.net) network, and the UVI values were obtained by UV irradiances measured by a Brewer spectrophotometer. The dataset covers a period of 11 years, from 2010 to 2020, in the spring-summer months (March to September). In the selected months, UVI at solar zenith angles (SZA) smaller than 40° are analyzed. For SZA>40°, the uncertainty on the irradiances measured by the Brewer increases due to effects such as stray light (Bais and Zerefos, 1996) and angular response error (Antòn et al., 2008). Therefore, an enhancement of the estimated error of UVI, which is about 4-5%, (Schmalwieser et al., 2017) is also expected. This could affect the identification of its variation caused by the aerosol effect.

2. Data

2.1 Measurement site

Rome is a large urban site, with about 3 million inhabitants, located 25 km east of the Tyrrhenian Sea, in the middle of an undulating plain. The atmosphere is affected by urban emissions as well as by semi-rural particulates and, especially during the spring and summer seasons, by sea breeze and long-range desert dust advection from the Saharan region (e.g., Ciardini et al., 2012, Di Bernardino et al., 2021). Long-term measurements of aerosol physical and optical properties, columnar ozone content and UV irradiance (290 -325 nm) are carried out in Rome, on the roof of the Physics Department of Sapienza University (41.9°N, 12.5°E; altitude 75m), in the central sector of the city. This site since 2019 is part of the BAQUNIN project (Iannarelli et al, 2021).

2.2 Sun-sky radiometer measurements

Aerosol properties are retrieved from observations taken in clear sky conditions by the sun-sky radiometer PREDE/POM model 01 (hereafter called POM). It is a narrow band filter photometer able to perform measurements of direct solar and diffuse sky irradiances within a narrow field of view of 1° at selected wavelengths (315, 340, 400, 500, 675, 870, 940 and 1020 nm). The measurement schedule includes direct irradiance observations every 1 minute and diffuse (almucantar, at 24 scattering angles in the range [0 –180°]) irradiances observations every 10 minutes. The 315 and 940 nm channels are mainly used to retrieve ozone and water vapor columnar content, whereas the other ones provide information on aerosols. The filter at 315 nm, which is characterized by a low transmittance, was replaced with one centered at 340 nm in May 2016. This instrument is part of the European Skynet Radiometer network (ESR, Campanelli et al., 2012; www.euroskyrad.net) that is a regional subnetwork of SKYNET (Nakajima et al., 2021); it has been operating in Rome since 2010 up to present. Calibration

is performed monthly by the Improved Langley method (Campanelli et al., 2007), a well-tested "on-site" procedure that allows to frequently check the instrument status.

2.3 Brewer measurements

Brewer MkIV spectrophotometer with the serial number 067 has been operating at the Solar Radiometry Observatory of the Physics Department of Sapienza University of Rome since 1992. Total column ozone have been recorded since 1992 whereas the spectral UV irradiance have been performed by the same instrument since 1996. This instrument is part of the European Brewer Network (EUBREWNET) and since 2019 has become part BAQUNIN project (Iannarelli et al, 2021).

The Brewer Mk-IV is a single monochromator spectrophotometer specifically designed to retrieve the total column ozone by measuring solar direct irradiances at selected UV wavelengths in the ozone absorption spectrum (Siani et al., 2018) and nitrogen dioxide in the visible part of the spectrum (Diémoz et al., 2021). The accuracy of direct-sun measurements of total ozone taken with a well-maintained Brewer spectrophotometer is 1% (Vanicek, 2006). The consistency among different instruments is ~1% (Redondas et al., 2018). The Brewer also measures global spectral irradiances from 290 nm to 325 nm with a step of 0.5 nm and a spectral resolution of about 0.6 nm. UV spectral scans are performed at Rome every 30 min throughout the day. The performance of the Brewer instrument for UV measurements was controlled every two years till 2014 through intercomparisons to the traveling reference QASUME UV spectroradiometer operated by Physykalish Meteorologisches Observatorium Davos/ World Radiation Centre (Gröbner et al., 2005). The mean ratio of Brewer integrated solar UV irradiances to QASUME is within +3% (see https://www.pmodwrc.ch/en/world-radiation-center-2/wcc-uv/). Thereafter, the UV calibration has been carried out by IOS using 1000 W lamps which are traceable to the National Institute of Standard and Technology - NIST, Maryland, USA, and regularly compared to QASUME (Siani, et al., 2013).

2.4 Particulate Matter samples collected at the surface

Results from an intensive field campaign (URBan Sustainability Related to Observed and Monitored Aerosol – URBS ROMA, Campanelli et al., 2012) conducted in the period June – July 2011 in the same location and aimed to determine the aerosol direct radiative effect at the surface, are also shown to provide additional information on the aerosol properties at Rome during a summer season, and to demonstrate the soundness of the column retrievals. PM_{10} (particulate matter with diameter smaller than 10 micrometers) samples were collected by using a dual channel sampler (HYDRA Dual Sampler, FAI Instruments, Fonte Nuova, Rome, IT) equipped with Teflon membrane filters and quartz fiber filters,

135 respectively on the two sampler's channels. The PM$_{10}$ mass concentration was measured on Teflon filters

136 by gravimetry using an automated microbalance.

137

138 **3. Methodology**

139 **3.1 Sun-sky radiometer retrieval method**

140 Skyrad_MRIv2. pack (Kudo et al., 2021), one of the official computer codes employed in the SKYNET

141 network, was used to retrieve the aerosol optical properties from the normalized radiance, which is the

142 ratio between the solar diffuse radiance and direct solar irradiance, at all available wavelengths. The

143 expected uncertainty in the retrieval products at near-ultraviolet, visible, and near-infrared wavelengths

144 is less than 0.04 for AOD, and less than 0.05 for SSA. The retrievals by Skyrad MRIv2 have been

145 previously validated based on in-situ measurements and radiative closure at the ground (Kudo et al.,

146 2021; Fasano et al., 2021a). A detailed comparison with the retrievals from a co-located AERONET

147 photometer operating at the BAQUNIN super-site is in preparation. The cloud screening was performed

148 based on the measurement of the fitness (f$_{obs}$) parameter introduced by Kudo et al. (2021). In order to

149 relate the UV Index to the aerosol optical properties, these latter have to be determined at a wavelength

150 as close as possible to the one corresponding to the maximum of the erythemally-weighted solar

151 spectrum (usually <320 nm, depending on the solar zenith angle). The shortest wavelength at which

152 reliable observations are available from the POM operating in Rome is 340 nm. Measurements at this

153 wavelength were started in 2016 ("dataset 2"), while the shortest wavelength was 400 nm prior to that

154 date ("dataset 1"). Hence, to increase the length of the aerosol dataset at the shortest measured

155 wavelength and cover a larger overlapping period with the UVI series from the Brewer, we developed a

156 new physically-based method (described below) to extrapolate the aerosol optical depth and aerosol

157 properties from longer wavelengths (400 nm and above) down to 340 nm for both dataset 1 and 2. Then,

158 to assess the accuracy of the method, we compare the outcome of this extrapolation with the retrieval

159 obtained using all available wavelengths, including 340 nm (period dataset 2). Based on the very good

160 results of such a comparison (Sect. 4.1), we always use the extrapolated data set throughout the period

161 analyzed here for consistency. Replacing the retrievals based on observations at 340 nm (in the few

162 periods when they are available) with the extrapolation is therefore not expected to affect the findings

163 of this study.

164 The extrapolation is performed using the Aerosol Optical Properties (AOP) program included in the

165 Skyrad MRIv2 package. AOP is able to calculate the aerosol optical properties at arbitrary wavelengths

166 from the results of the Skyrad inversion, using the same kernels as in the retrieval. For example, it is

167 normally used to interpolate the aerosol properties to the lidar wavelengths. The optical properties are

168 calculated by the procedure described by Kudo et al. (2021), i.e. from the retrieved volume size

distribution (VSD) and complex refractive index. The real (RRI) and imaginary (IRI) part of the refractive index are interpolated in the log–log space. In the default AOP operation, the RRI and IRI at the shortest/longest available wavelengths are used when properties at wavelengths beyond the measured interval are requested. However, in the present study we further modified the code to allow extrapolation outside the measurement interval. The limitations of this approach are discussed in the next sections. Hence, the aerosol products considered in this study are: AOD_{340}, SSA_{340}, Absorption Aerosol Optical Depth ($AAOD_{340} = AOD_{340}*(1-SSA_{340})$) and Ångström exponent calculated from the AOD at 340 and 500 nm (Ae_{340_500}) to infer the AOD wavelength dependence in that spectral range.

3.2 Brewer retrieval method

Spectral UV irradiances, measured by the Brewer spectrophotometer in clear sky conditions (no clouds obscure the sun), selected according to the Alexandrov et al. (2004) methodology, were used to retrieve the UV index (UVI). The UVI was introduced in Canada in 1992 (Fioletov, 2010) to represent the potentially harmful effects of UV radiation in a simple form. UVI is a unit-less quantity determined by multiplying the erythemally weighted UV irradiances (in $W\,m^{-2}$) over the range 280-400 nm by $40\,m^2 W^{-1}$ (COST-713, 2000). UVI values are grouped into exposure category expressing the risk for unprotected skin to Sun exposure. Typically at mid-latitudes, UVI values at noon vary from 0 to 10, but highest UVI values (a peak of 12.3 at Plateau Rosà, 3500 m a.s.l., in Valle d'Aosta Region, Italy) are experienced at high altitudes (e.g., Casale et al., 2015) or at lower latitude sites.

The spectral irradiances were processed using the SHICrivm software version 3_075 (Slaper et al., 1995) to check for any spectral wavelength shift and spectral anomalies (Slaper et al, 1995) in the UV data. Furthermore, the software allowed to obtain the biologically effective UV irradiance by weighting the solar irradiances with the erythemal action spectrum (C.I.E., 1999). Since the Brewer MKIV spectrophotometer measures spectral irradiances up to 325 nm, the non-measured part of the UVA spectrum needed for the calculation of UVI was extrapolated by the same software. Based on considerations for similar corrections in the Brewer operating software (Fioletov et al., 2004), we estimate an additional contribution (<2%) to the overall uncertainty in the UV index value for solar zenith angles <70° due to this extrapolation.

Total ozone values (O_3) from direct-sun measurements were generated by using the Brewer Processing Software, applying the rejection criteria on ozone values less than 100 DU and greater than 500 DU (Siani et al., 2018). Yet, individual total ozone values were discarded when standard deviation is above 2.5 DU and ozone air mass is above 3.5 (the ozone air mass is defined as the ratio of the actual ozone path length taken by the direct solar beam to the analogous vertical ozone path when the Sun is overhead from the surface to the top of the atmosphere).

203

3.3 PM samples chemical analysis

Chemical characterization of the PM_{10} samples collected during the URBS campaign was carried out according to the method reported in Perrino et al. (2009). Briefly, elements were determined on Teflon filters by X-ray fluorescence (XRF); then the filters were water-extracted and analyzed for their ionic content by ion chromatography (IC); elemental and organic carbon (EC and OC) were detected on quartz filters by thermo-optical analysis (NIOSH-QUARTZ temperature protocol). This overall analytical procedure allows the determination of each individual component typically accounting for more than 1% of the PM_{10} mass (macro-components: Si, Al, Fe, Na, K, Mg, Ca, chloride, nitrate, sulfate, ammonium, elemental carbon, organic carbon) and to obtain the mass closure.

PM_{10} macro-components can be grouped into five clusters to estimate the contribution of the main macro-sources: SOIL, SEA, SECONDARY INORGANICS, ORGANICS, and TRAFFIC. Details about the algorithms are reported in Perrino et al. (2014). The contribution of SOIL was calculated by adding the concentration of those elements (considered as metal oxides) generally associated with mineral dust: Al, Si, Fe, the insoluble fractions of K, Mg, and Ca (calculated as the difference between XRF and IC determinations), calcium and magnesium carbonate (calculated as the sum of soluble calcium multiplied by 1.5 and soluble magnesium multiplied by 2.5); SEA was estimated from the sum of Na^+ and Cl^-, multiplied by 1.176 in order to take into account minor sea-water components; SECONDARY INORGANICS were calculated as the sum of nitrate, ammonium and non-sea-salt sulphate; the contribution of road TRAFFIC was estimated by adding elemental carbon to an equivalent amount multiplied by 1.1 in order to consider the contribution of primary organic matter that can be adsorbed on particles surface; the remaining organic carbon, multiplied by 1.6 to take into account non-C atoms, constituted the ORGANICS and included both secondary organic species and primary components.

226

3.4 Optical properties of surface aerosol from a radiative transfer model

Rstar is a radiative transfer model (Nakajima and Tanaka 1986) able to simulate the radiation fields in the atmosphere-land-ocean system in the wavelength range $0.17 - 1000$ μm. Eight fundamental materials (water, dust-like, sea salt, volcanic ash, yellow sand, ice, water-soluble, soot and 75%H_2SO_4) are considered to assemble a three component internal mixture for each of the ten particles model types (Water, dust-like, volcanic-ash, rural, urban, yellow sand, ice, soot, 75%H_2SO_4, sea spray, tropo).The imaginary parts of refractive index of each fundamental material in the Rstar model were used as reference values and helped to understand the variety of absorption capability of the PM_{10} macro-components concentration in the atmosphere over Rome.

236

3.5 Assessment of the dependence of UVI on the aerosol optical properties

To discern the dependence of UVI on the aerosol characteristics, the influence produced by solar zenith angle total column of ozone, and orbital parameters (varying Earth-Sun distance) must be minimized. Therefore, firstly the UVI was corrected for the variation of the Earth-Sun distance and values were reduced to the mean Sun-Earth distance (Madronich, 1993). Secondly, only data at two values of SZA30° (±1°) and 40°(±1°) were selected. This criterion excludes data related to autumn and winter seasons , when the solar zenith angle is always higher than 40° in Rome. Thirdly, the UVI dependence on total O_3 has been removed. This correction has been implemented using the Radiation Amplification Factor (RAF) and scaling the UVI to the total ozone daily average value for the day with the lowest AOD_{340} recorded in the entire dataset (283 DU on July 8, 2014). In fact, the effect of ozone on the erythemal UV irradiance may be described as suggested by Madronich (1993) and Booth and Madronich (1994):

$$\frac{E^*}{E} = \left(\frac{O_3}{O_3^*}\right)^{RAF},\tag{1}$$

where E and E* are two UV irradiances observations, and O_3 and O_3^* their corresponding total ozone amounts.

Similarly, it is possible to apply the above relationship to UVI:

$$UVI^* = UVI\left(\frac{<O_3>}{O_3^*}\right)^{RAF},\tag{2}$$

where $<O_3>$ is the daily ozone average value, O_3^* is the daily ozone average value during the day with the minimum average AOD_{340}, and RAF is assumed to be equal to 1.25, according to di Sarra et al. (2002). In that study the authors (Figure 8) retrieved values of RAF after correcting for the influence of co-varying aerosol optical depth and they found the values between 1.0 and 1.2 at 30° and 40° solar zenith angles when considering all aerosol conditions. As discussed in the paper, these values are affected by different processes (the wavelength dependence of the aerosol sensitivity, the interdependence between ozone and aerosol, possibly through increased ozone absorption following enhanced scattering by aerosols, ozone and aerosol vertical distributions). The values of 1.25 was derived from UVSPEC radiative transfer model calculations (Edme et al., 2016) where the aerosol amount was kept fixed. This value is also in agreement with various other determinations of the ozone RAF (e.g., De Luisi and Harris, 1983; McKenzie et al., 1991; Kerr and McElroy, 1993). However, a sensitivity study of UVI* on RAF variation from 1 to 1.25 has been performed over all the dataset showing an average decrease of UVI* by about 1.4%, that is within the declared uncertainty of 4-5%, (Schmalwieser et al., 2017).

268   To point out the possible effect of aerosol optical characteristics measured at 340 nm on UVI^*, AOD_{340},

269   SSA_{340}, $AAOD_{340}$ and $Ae_{340-500}$ were analyzed as function of UVI^* at the two fixed solar zenith angles,

270   associating estimations of aerosol parameters and UVI* made within ±5 minutes.

271

272   **4. Results**

273   **4.1 Validation of the method to extrapolate the aerosol properties to 340 nm**

274   Figure 1 shows a comparison of the AOD and SSA extrapolated at 340 nm by AOP (from wavelengths

275   of 400 nm and above) and retrieved by Skyrad MRIv2 using all wavelengths (including 340 nm), for the

276   period 2017-2020 (dataset 2). The discrepancies are well within the estimated uncertainties for both

277   AOD_{340} and SSA_{340}. Regarding the latter, it is possible that the extrapolation leads to a slight

278   overestimation due to neglecting organic aerosols in the atmosphere, that are instead present in Rome as

279   found during the URBS campaign (Sect. 4.3). Indeed, the organic compounds are characterized by a

280   larger absorption in the UV than in the visible range (Massabò et al., 2015).

281   To remove this residual discrepancy, thus taking the likely effect of organics into account, we further

282   corrected the extrapolated data (AOD and SSA) by applying a simple offset/slope correction derived

283   from the linear regression of AOP (y) vs Skyrad (x, with $y = 0.12 + 0.89x$). By definition, this brings the

284   AOP results to overlap to the Skyrad MRI retrievals on average, for the selected period. This correction

285   assumes that the average relationship found for the 2017-2020 period also stands for the previous years.

286   To verify this hypothesis, we again compare this optimized extrapolation to the real Skyrad retrievals in

287   a different period (May-December 2016), when measurements at 340 nm are also available. Negligible

288   differences are obtained, on average, even for this period (dAOD < 0.006 and dSSA < 0.01, not shown),

289   hence demonstrating the robustness of the procedure.

290

291
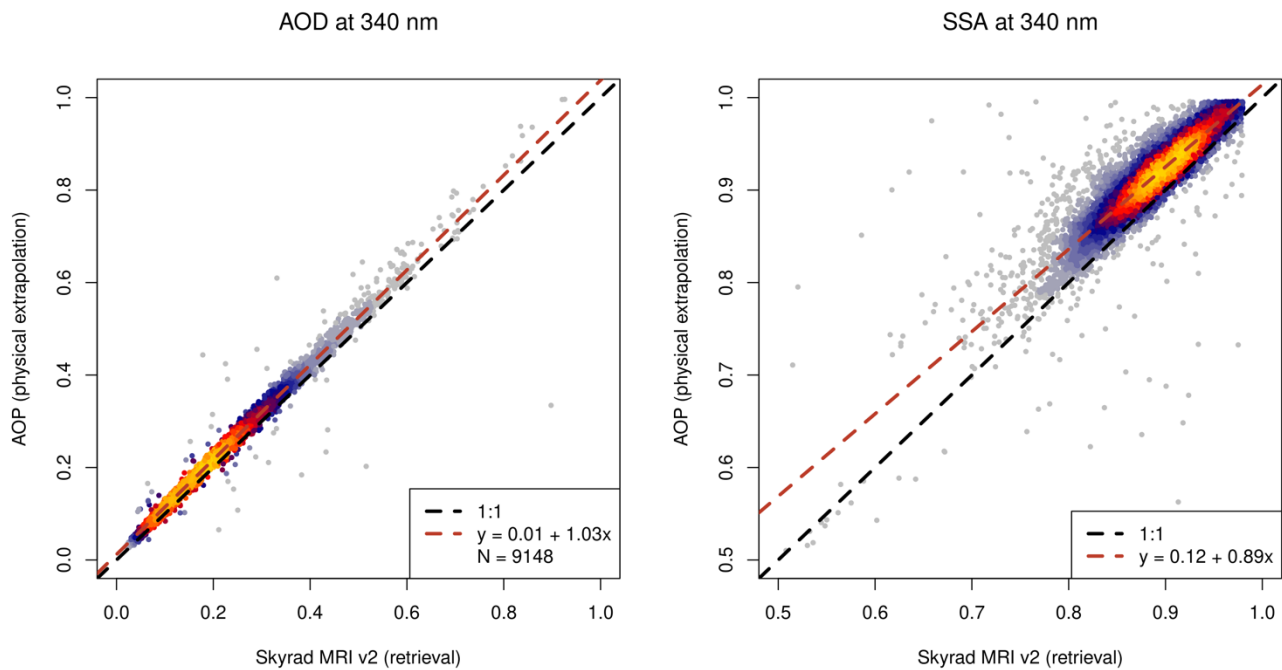
Fig. 1: Comparison of the AOD (left panel) and SSA (right panel) at the wavelength of 340 nm retrieved from Skyrad MRIv2 using measurements at all wavelengths as input and the physically-based extrapolation from the visible-IR (>400 nm) to 340 nm based on the AOP program. Colors represent the density of the points based on a two-dimensional Kernel Density Estimation (Venables and Ripley, 2013). Data refer to the period 2017-2020, i.e. a period when measurements in the 340-nm channel were available.

298

4.2 UVI dependence on aerosol optical parameters

The analyzed dataset covers the period March – September from 2010 to 2020 (for the last year the series ends in August). Figure 2 shows monthly averages of AOD_{340}, SSA_{340}, and $Ae_{340-500}$ for the period under study. Monthly means of SSA_{340} vary between a minimum value of 0.84±0.04 (observed in March 2010) and a maximum of 0.94±0.01 (observed in June 2015). AOD_{340} monthly mean values range between a minimum of 0.15±0.08 (in May 2019) and a maximum of 0.43±0.25 (in June 2015). $Ae_{340-500}$ varies between 0.45±0.37 (in March 2018) and 1.34±0.19 (in June 2015). The total ozone content values are also plotted in Figure. 2. The seasonal ozone behavior is typical of mid-latitude sites, with highest values measured in spring and particularly in April 2010 (385 DU) and the minimum in September 2011 (292 DU).

During June-July 2011 the PM_{10} chemical analyses show an average contribution over the entire sampled mass of about 29% of SOIL, 6% of SEA, 23% of SECONDARY INORGANIC, 28% of ORGANICS and 9% of TRAFFIC components. The absorption capability of these components is very different: in the Rstar radiative transfer model at 336 nm the imaginary part of refractive index varies from low values

(weak absorption) of $4.02*10^{-7}$ for marine aerosol (sea salt) and $1.00*10^{-8}$ for 75%H2SO4 (characterizing SECONDARY INORGANICS fraction) to a maximum of $4.70*10^{-1}$ for soot (characterizing the TRAFFIC contribution). It is therefore expected that the modulation of the concentration of these co-existent materials, can strongly affect the absorption capability of the atmosphere over Rome.
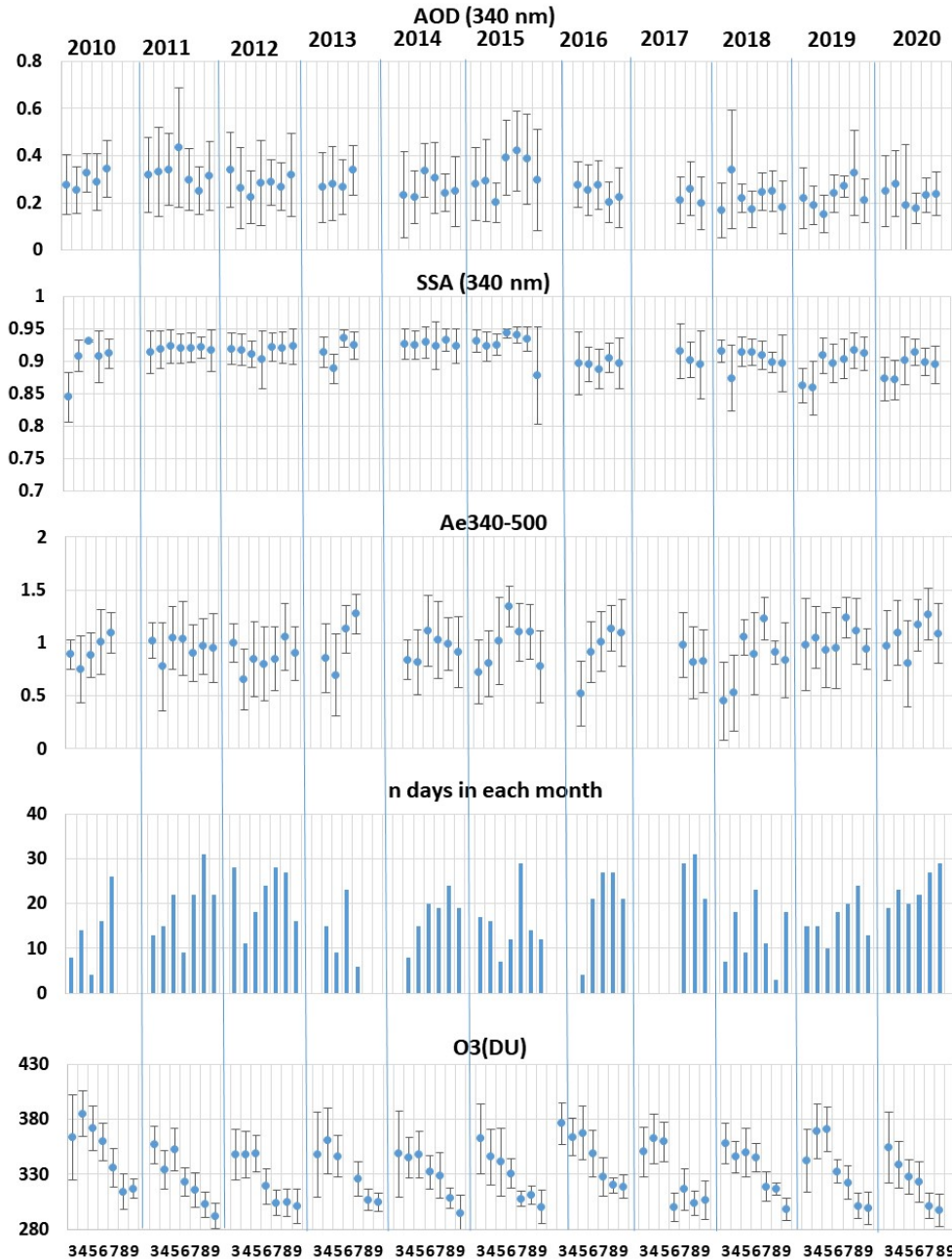
Figure 2: Monthly averages of AOD_{340}, SSA_{340}, $Ae_{340-500}$ and total O_3 for each year from 2010 to 2020. The number of points refers to the available daily mean data used in the calculation of the aerosol parameters monthly means. Error bars are the standard deviation that for SSA can be lower compared to the reported 0.05 error on SSA retrieval.

324   A regression analysis of the daily means of SSA_{340}, AOD_{340}, $AAOD_{340}$ and $Ae_{340-500}$ and the percentage
325   contribution of each chemical component, has been performed in order to check whether the optical
326   properties retrieved over the whole column and the chemical composition of samples collected at the
327   surface are linked. Scatter plots of SSA_{340} and $AAOD_{340}$ versus the fraction of SOIL component
328   contained in PM10 (Figure 3b, d) exhibit a reasonable correlation (R^2= 0.49 and 0.31 respectively)
329   showing an increase of the absorption capability in the atmosphere (lower SSA_{340} and higher $AAOD_{340}$
330   values) with the enhancement of the SOIL contribution. A weaker correlation is found between Ae_{340-}
331    $_{500}$ and the percent amount of ORGANICS and SECONDARY INORGANICS contributions (R^2= 0.35
332   and 0.22 respectively) highlighting that an enrichment of these particulates sampled at ground level may
333   be associated with higher values of $Ae_{340-500}$ due to the presence of smaller particles in the atmosphere
334   (Figure 4c). SECONDARY INORGANICS seems also to be weakly correlated with AOD_{340} in Rome.
335
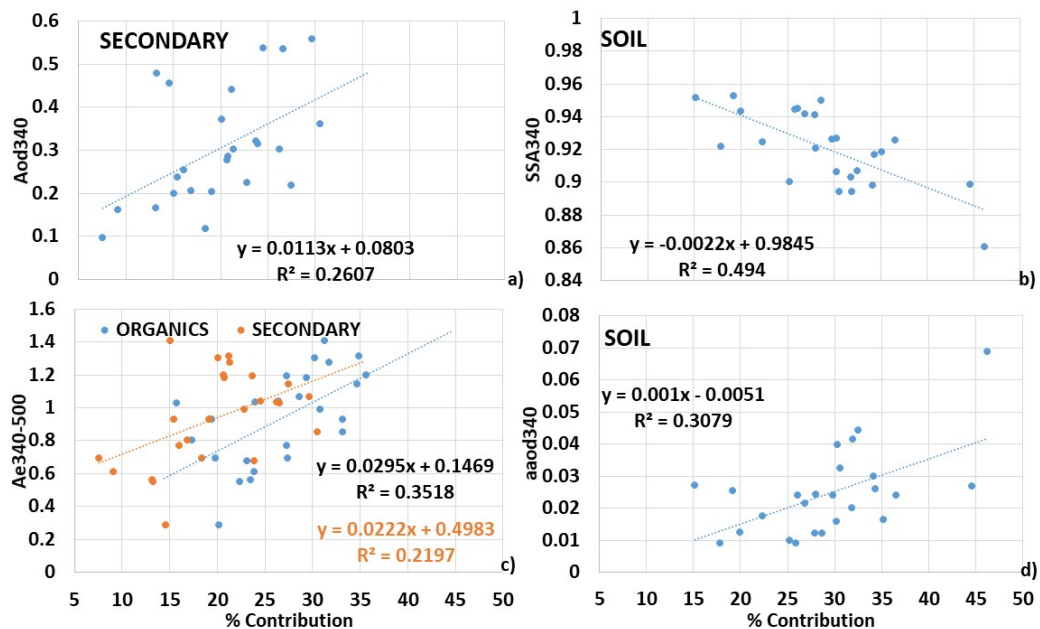
337   Figure 3. Behaviour of AOD_{340}, SSA_{340}, $Ae_{340-500}$ and $AAOD_{340}$ versus the percentage contribution of
338   some components as retrieved during the URBS campaign.
339

340   In order to point out the possible effect of aerosol optical characteristics measured at 340 nm on UVI[*],
341   the AOD_{340}, SSA_{340}, $AAOD_{340}$, and $Ae_{340-500}$, were analyzed as function of UVI[*], at the two selected
342   values of solar zenith angle. Figure 4 shows the frequency distributions of the number of measurements
343   per month for each of the two angles. SZA=30° is more representative of the warmest months, whereas
344   40° covers a wider period.
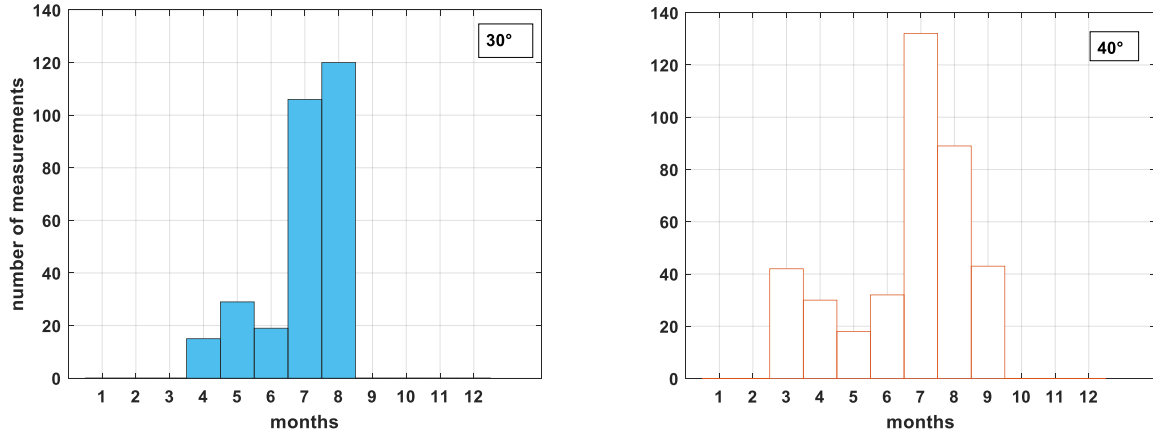
Figure 4: Number of measurements available for each zenith angle.

The dependency of UVI* on AOD_{340}, SSA_{340}, $AAOD_{340}$ and Ae_{340_500} for 30° and 40° solar zenith angles is shown in Figure 5, colored for different values of SSA_{340} or AOD_{340}. Slopes, intercepts and correlation coefficients R^2, are shown in Table I. The slope retrieved for UVI* versus AOD corresponds to the UVI radiative forcing efficiency, i.e., the change in UVI produced by a unit change in AOD.

It is worthwhile mentioning that the UVI "effective" wavelengths are around 305-310nm depending on solar elevation, whereas aerosol properties are here retrieved at 340nm. Since AOD_{305} is theoretically higher than AOD_{340} for the same instant and the relationship between $AAOD_{305}$ and $AAOD_{340}$ depends on SSA spectral behavior in the UVB, the obtained results in Figure 5 and table I could be partly affected by the spectral behavior of both AOD and SSA in the 305-340 nm range. A slight decreasing trend of UVI* when increasing AOD_{340} is evident at the smaller solar zenith angle, in agreement with what is found by previous studies (di Sarra et al., 2008; Antón et al., 2011). For the other parameters no dependence is visible from this first analysis. To investigate in more detail the possible effects on UVI* caused by particles dimensions and atmospheric absorption capabilities, the entire dataset was divided in two groups of Ae_{340_500} values, respectively below and above 1, and in two groups of SSA_{340} values, smaller and larger than 0.9, respectively. The values separating the different groups were determined according to the frequency distributions of the two variables for the entire investigation period, shown in Figure 6; they are the median values of the distributions. To understand if the extreme values of the distributions have a different impact on UVI*, also the first and fourth quartiles were considered as thresholds values for the SSA_{340} and $Ae_{340-500}$ datasets: i) smaller than 0.8 and greater than 1.2, for $Ae_{340-500}$ dataset; ii) smaller than 0.87 and larger than 0.93 for SSA_{340}. Scatter plots of UVI* versus the two variables, for each group, were performed and points with a distance greater than 2σ from the regression line (nout), with σ the standard deviation of the residuals, were rejected for the final linear fit. The

dependence of UVI* on AOD for the classes of $Ae_{340-500}$ separated by median value, is shown in Figure 7, colored for different values of SSA_{340}, and statistical results for all the classes are reported in Table I. At 30° the slope is greater for smaller values of $Ae_{340-500}$, both in the case of median and quartiles thresholds (-3.27 and -3.02 respectively), similarly to what found by Antón et al. (2011), and the correlation coefficients R^2 are the highest. Small values of Angstrom exponents are due to the presence of coarse particles, that in Rome are generally related to the presence of Saharan dust, more absorbing in the UV than VIS regions.

Smaller particles show a smaller forcing efficiency, despite the presence of organic aerosol likely absorbing in the UV range (Fig. 3). In fact in the case of $Ae_{340-500}$ greater than 1. 0, which according to the analysis from the URBS campaign is likely related to concentrations from 15% to 35% of ORGANICS and SECONDARY INORGANICS fractions (Figure 3c), smaller values of slope (-1.28 and -1.34) and R^2 are visible. These small particles are able to reduce the UVI* by about 1.0 when AOD_{340} reaches values of 0.7. A similar dependency on the Ångström exponent was found by di Sarra et al. (2008) when considering the forcing efficiency over the whole shortwave spectral range.

At 40° SZA the slope is reduced with respect to 30°, as expected. Slightly larger (negative) slopes are found at 40° for $Ae_{340-500}$ values > 1.0, however these differences are not significant compared to the combined uncertainty of the slopes and might have been introduced by statistical sampling only.

Figure 8 shows the scatter plots of UVI* vs AOD_{340} for SSA_{340} <0.9 (top) and $SSA_{340} \geq 0.9$ (bottom), with a colour scale for different values of the Ångström exponent at the two zenith angles. Less absorbing particles (SSA_{340} > 0.9) shows similar slopes at 30° and 40°. The slopes increase in the case of a more absorbing atmosphere, in agreement with the findings by Antòn et al. (2011) in Granada, Spain, where, as expected, stronger aerosol absorption leads to a large surface forcing efficiency. At 30°SZA slopes reache values of -2.68 and -2.52 in the case of median and quartiles thresholds, respectively. According to the results from the URBS campaign (Figure 4b, d) the absorption capability (SSA_{340} and $AAOD_{340}$) in Rome is correlated to the increase of the SOIL concentration, therefore it could be inferred that the greater is this component in the atmosphere the larger is the radiative forcing efficiency. The slopes are again greater at 30° compared with the results at 40°.

			SZA =30°			SZA =40°		
		UVI* vs:	Slope	Intercept	R^2	Slope	Intercept	R^2
	All data	AOD_{340}	-1.91±0.23	8.72	0.21	-1.00±0.15	6.21	0.11
		$AAOD_{340}$	-9.57±1.76	8.48	0.10	-5.51±1.12	6.09	0.06
		SSA_{340}	-0.79±0.71	8.94	0.01	-0.66±0.53	6.52	0.004
	$Ae_{340-500} < 1.0$	AOD_{340}	-3.27±0.32	8.87	0.58	-1.17±0.20	6.17	0.23

median	$Ae_{340-500} \geq 1.0$	AOD_{340}	-1.28±0.18	8.55	0.27	-1.36±0.12	6.37	0.41
quartiles	$Ae_{340-500} < 0.8$	AOD_{340}	-3.02±0.35	8.68	0.66	-0.96±0.25	6.07	0.15
	$Ae_{340-500} \geq 1.2$	AOD_{340}	-1.34±0.22	8.63	0.33	-1.56±0.15	6.49	0.55
median	$SSA_{340}<0.9$	AOD_{340}	-2.68±0.28	8.92	0.47	-1.65±0.18	6.45	0.34
	$SSA_{340}\geq 0.9$	AOD_{340}	-1.08±0.19	8.47	0.21	-1.05±0.13	6.18	0.29
quartiles	$SSA_{340}<0.87$	AOD_{340}	-2.52±0.38	8.87	0.48	-1.83±0.22	6.48	0.46
	$SSA_{340}\geq 0.93$	AOD_{340}	-0.97±0.26	8.50	0.20	-0.78±0.17	6.12	0.22

398

399 Table I: Slope, intercept and determination coefficient values for the linear fit of UVI* vs AOD_{340},

400 $AAOD_{340}$ and SSA_{34} for different cases and the two zenith angles

401
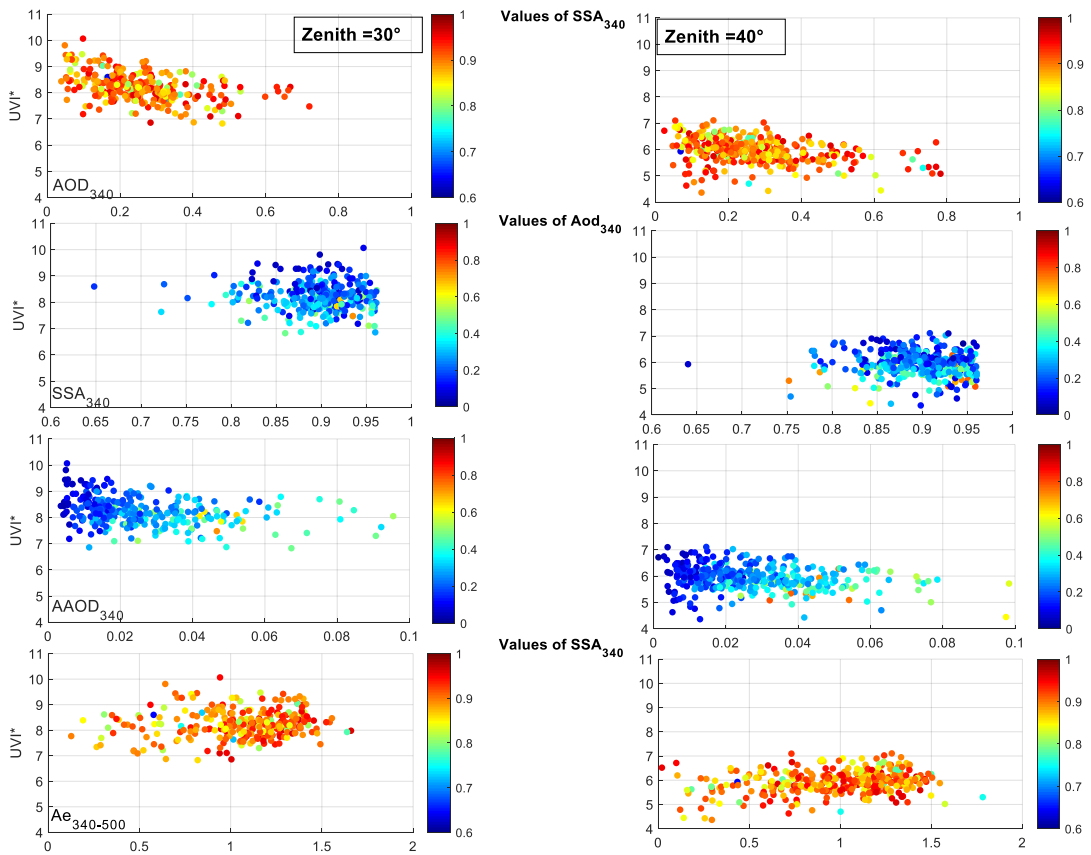
402

403 Figure 5 Scatter plot of UVI* vs AOD_{340} (top), SSA_{340} (second raw), $AAOD_{340}$ (third raw) and $Ae_{340-500}$

404 (bottom) for solar zenith angles of 30° (left) and of 40° (right). The colors represent the values of SSA_{340}

405 (first, and fourth rows) and AOD_{340} (second and third rows).
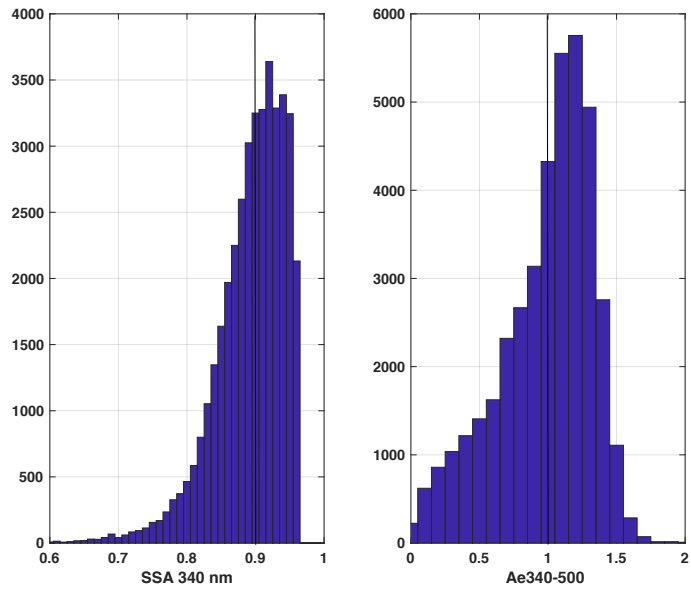
Figure 6. Frequency distributions of the values of SSA_{340} (left) and $Ang_{340-500}$ (right) for the entire investigation period. The median values used as threshold values to separate the different classes are highlighted with vertical black lines.
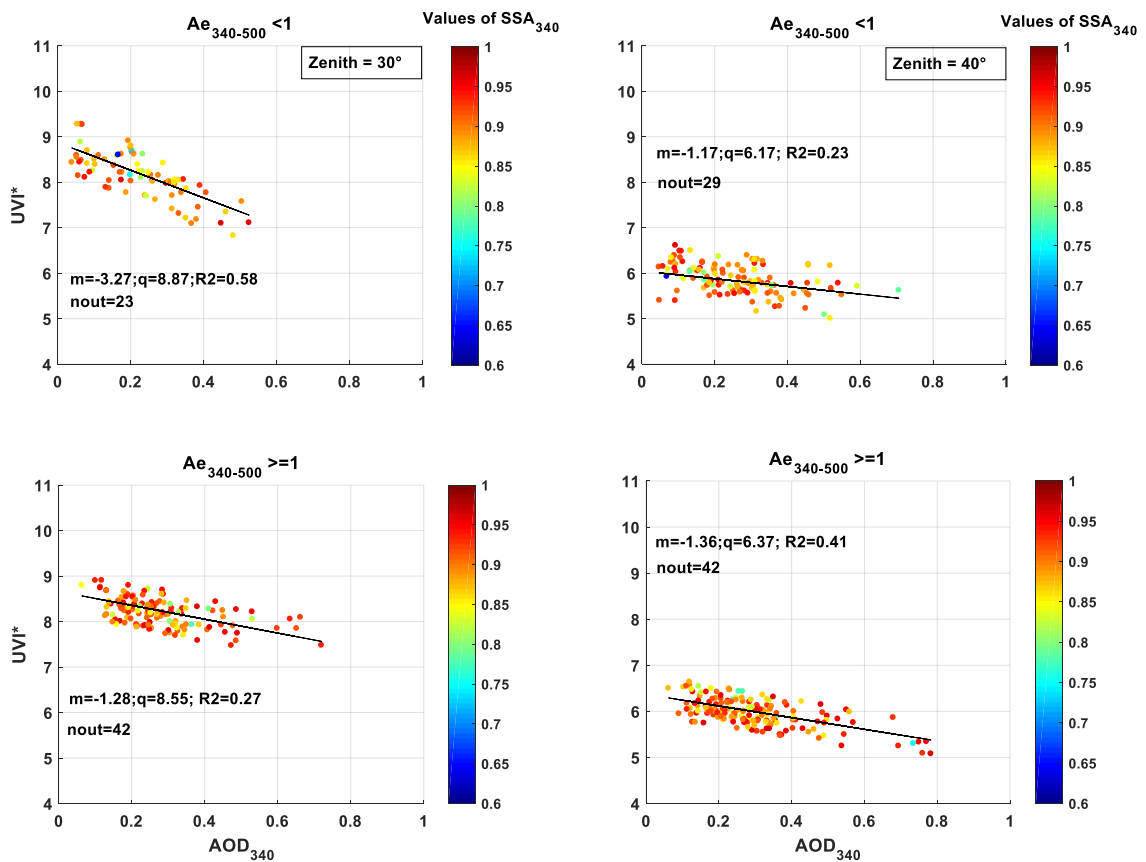
412 Figure 7 scatter plot of UVI* vs AOD$_{340}$ for two groups of Ang$_{340-500}$ values and two solar zenith angles.
413 The colors represent the values of SSA$_{340}$. "nout" is the number of rejected outliers. "m" is the slope and
414 "q" is the intercept value.

415
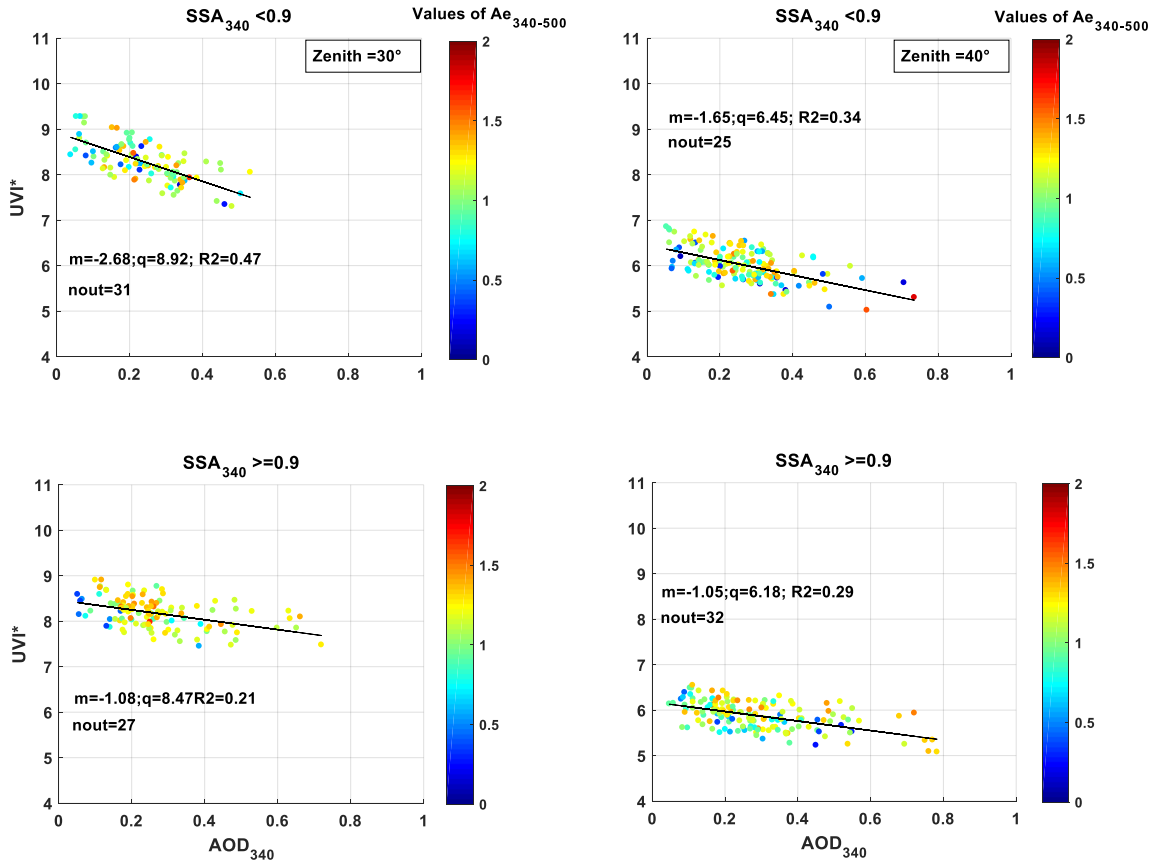
416
417 Figure 8 scatter plot of UVI* vs AOD$_{340}$ for two groups of SSA$_{340}$ values and two solar zenith angles.
418 The colour scale refers to the values of Ang. "nout" is the number of rejected outliers. "m" is the slope
419 and "q" is the intercept value.

420

5. Conclusions

422 The aerosol optical properties in the urban area of Rome were retrieved for a period of 11 years, in the
423 months from March to September 2010-2020, when also co-located surface measurements of the spectral
424 UV irradiance were available. The impact of AOD and SSA at 340 nm, and Ångström exponent
425 calculated at 340-500 nm on the UV Index has been analyzed. A new physically-based method was
426 developed to extrapolate the aerosol optical properties to the UV range when only visible to infrared
427 measurements were available. The method was validated based using data collected at all wavelengths
428 and was applied to the period when measurements at 340 nm were not available. The dependence of
429 UVI*, corrected for total ozone changes and scaled at the mean Sun-Earth distance, was studied with

respect to AOD_{340}, SSA_{340}, $AAOD_{340}$ and $Ae_{340-500}$. Data at two fixed values of the solar zenith angle (30° and 40°) were selected in order to identify possible effects of the aerosol optical characteristics on UVI^*. A slight decreasing trend of UVI^* when increasing AOD_{340} is evident at the smaller solar zenith angle, with the slope corresponding to the UVI^* radiative forcing efficiency, i.e. the change in UVI^* produced by a unit change in AOD. For the other parameters no dependence is visible.

To investigate in more detail the possible effects on UVI^* caused by particles dimensions and atmospheric absorption capabilities, the entire dataset was divided in two groups of Ae_{340_500}, below and above 1, and in two groups of SSA_{340}, smaller and larger than 0.9, where the thresholds are the median values of the two data distributions.

The forcing efficiency was found greater for lower zenith angle and smaller values of $Ae_{340-500}$ both in the case of median and quartiles thresholds. Small values of Angstrom exponents are related to the presence of coarse particles, that in Rome are generally linked to the presence of Saharan dust in the atmospheric column, more absorbing in the UV than VIS regions.

More absorbing particles ($SSA_{340} < 0.9$) showed a larger forcing efficiency at smaller zenith angles. According to the results from the URBS campaign in Rome the absorption capability is correlated to the increase of the SOIL fraction, therefore it could be inferred that the greater is this component in the atmosphere the larger is the radiative forcing efficiency.

Data availability

All raw data can be provided by the corresponding authors upon request.

Author contributions

MC, HD and AdS wrote the manuscript draft; AdS MC, HD, AI, AS, GF, LT analyzed the data; MC, AS, AI, GC, LT and MC, performed the measurements; RK developed the model and supported the authors to its use; GC, LT, PS and SD reviewed and edited the manuscript.

Competing interests

The authors declare that they have no conflict of interest.

References

Alexandrov, M. D., Marshak, A., Cairns, B., Lacis, A. A, and Carlson, B. E.: Automated cloud screening algorithm for MFRSR data, Geophys. Res. Lett., 31, L04118, doi:10.1029/2003GL019105, 2004

Antón, M., Serrano, A., Cancillo, M.L., Vilaplana, J., Cachorro, V.E., and Gröbner J., 2008: Correction of Angular Response Error in Brewer UV Irradiance Measurements. J. Atmos. Oceanic Technol., 25, 2018–2027, https://doi.org/10.1175/2008JTECHA1040.1

Antón, M., Gil, J. E., Fernández-Gálvez, J., Lyamani, H., Valenzuela, A., Foyo-Moreno, I., Olmo, F. J., and Alados-Arboledas, L.: Evaluation of the aerosol forcing efficiency in the UV erythemal range at Granada, Spain, J. Geophys. Res. 116, D20214, doi:10.1029/2011JD016112, 2011

Bais, A. F. and. Zerefos, C. S: Solar UVB measurements with the double- and single- monochromator Brewer Ozone Spectrophotomete, Geophysical Research Letters, vol. 23, no. 8, pages 833-836, april 15, 1996

Campanelli, M., Estellés, V., Smyth, T., Tomasi, C., Martínez-Lozano, M. P., Claxton, B., Muller, P., Pappalardo, G.,Pietruczuk, A., Shanklin, J., Colwell, S., Wrench, C., Lupi, A.,Mazzola, M., Lanconelli, C., Vitale, V., Congeduti, F., Dionisi,D., and Cacciani, M.: Monitoring of Eyjafjallajoekull volcanic aerosol by the new European SkyRad users (ESR) sun–sky radiometernetwork, Atmos. Environ., 48, 33–45, 2012.

Campanelli M., C. Bassani, M. Cacciani, A.M. Siani , C. Perrino , S. Canepari , A. Di Sarra, R. Salzano, G.P. Casasanta , C. Tirelli , and V. Estelles: Direct effect of aerosol on incident solar radiation at the surface as a function of aerosol mixtures measured in the center of Rome, Geophysical Research Abstracts, Vol. 14, EGU2012-4820, 2012, EGU General Assembly.

Campanelli, M., Estellés, V., Tomasi, C., Nakajima, T., Malvestuto, V., and Martiínez-Lozano, J. A.: Application of the SKYRAD Improved Langley plot method for the in situ calibration of CIMEL Sun–sky photometers, Appl. Optics, 46, 2688–2702, 2007.

Casale, G.R., Siani, A.M., Diémoz, H., Agnesod, G., Parisi, A.V., Colosimo, A. Extreme UV index and solar exposures at Plateau Rosà (3500ma.s.l.) in Valle d'Aosta Region, Italy, Science of the Total Environment, 512-513, 622-630, 2015.

Casasanta, G., di Sarra, A., Meloni, D., Monteleone, F., Pace, G., Piacentino, S., and Sferlazzo D.: Large aerosol effects on ozone photolysis in the Mediterranean, *Atmos. Environ.*, **45**, 3937-3943, 2011.

497   Castro, T., Madronich, S., Rivale, S., Muhlia, A., and Mar, B.: The influence of aerosols on

498   photochemical smog in Mexico City, Atmos.Environ., 35, 1765–1772, 2001

499

500   Ciardini, V., Di Iorio T., Di Liberto L., Tirelli C., Casasanta G., di Sarra A., Fiocco G., Fuà D., Cacciani

501   M. : Seasonal variability of tropospheric aerosols in Rome, Atmospheric Research, Vol 118, 15 Nov.

502   2012, Pages 205-214 https://doi.org/10.1016/j.atmosres.2012.06.026

503

504   CIE: CIE S007/E-1998 Erythema reference action spectrum and standard erythema dose, Color Res.

505   Appl., 24, 158–158, https://doi.org/10.1002/(sici)1520-6378(199904)24:2<158::aid-col11>3.0.co;2-4,

506   1999

507

508   COST-713 Action. UV Index for the Public. European, Communities. Brussels, 27, 2000.

509

510   De Luisi, J. J., and Harris, J. M.: A determination of the absolute radiant energy of a Robertson-Berger

511   meter sunburn unit, Atmos. Environ., 17, 751–758, 1983.

512

513   Di Bernardino A., Iannarelli, A.M., Casadio, S., Mevi, G., Campanelli, M., Casasanta, G., Cede, A.,

514   Tiefengraber, M., Siani, A. M., Spinei, E., Cacciani, M.: On the effect of sea breeze regime on aerosols

515   and gases properties in the urban area of Rome, Italy, Urban Climate,Volume 37,2021,100842, ISSN

516   2212-0955,https://doi.org/10.1016/j.uclim.2021.100842.

517

518   Dickerson, R. R., Kondragunta, S., Stenchikov, G., Civerolo, K. L.,Doddridge, B. G., and Holben, B.

519   N.: The impact of aerosolson solar ultraviolet radiation and photochemical smog, Science,278, 827–830,

520   https://doi.org/10.1126/science.278.5339.827,1997

521

522   Diémoz, H., Siani, A. M., Casadio, S., Iannarelli, A. M., Casale, G. R., Savastiouk, V., Cede, A.,

523   Tiefengraber, M., and Müller, M.: Advanced NO2 retrieval technique for the Brewer spectrophotometer

524   applied to the 20-year record in Rome, Italy, Earth Syst. Sci. Data, 13, 4929–4950,

525   https://doi.org/10.5194/essd-13-4929-2021, 2021.

526

527   di Sarra A., Cacciani, M., Chamard, P., Cornwall, C., DeLuisi, J. J., Di Iorio, T., Disterhoft, P., Fiocco

528   G., Fua`, D., and Monteleone, F.: Effects of desert dust and ozone on the ultraviolet irradiance at the

529   Mediterranean island of Lampedusa during PAUR II Journal of Geophysical Research, Vol. 107, No.

530   D18, 8135, doi:10.1029/2000JD000139, 2002

531

di Sarra, A., Pace, G., Meloni, D., De Silvestri, L., Piacentino, S., and Monteleone, F.: Surface shortwave radiative forcing of different aerosol types in the Mediterranean, Geophys. Res. Lett., 35, L02714, doi:10.1029/2007GL032395, 2008.

535

Draxler, R. R., and. Hess, G. D, 1998: An overview of the HYSPLIT_4 modeling system for trajectories, dispersion, and deposition. Aust. Meteor. Mag., 47, 295–308

538

Dubovik, O. and King, M. D., 2000: A flexible inversion algorithm for retrieval of aerosol optical properties from Sun and sky radiance measurements," J. Geophys. Res., 105, 20 673-20 696.

541

Emde, C., Buras-Schnell, R., Kylling, A., Mayer, B., Gasteiger, J., Hamann, U., Kylling, J., Richter, B., Pause, C., Dowling, T., and Bugliaro, L.: The libRadtran software package for radiative transfer calculations (version 2.0.1), Geosci. Model Dev., 9, 1647–1672, https://doi.org/10.5194/gmd-9-1647-2016, 2016.

546

Fasano, G., Diémoz, H., Fountoulakis, I. et al. Vertical profile of the clear-sky aerosol direct radiative effect in an Alpine valley, by the synergy of ground-based measurements and radiative transfer simulations. Bull. of Atmos. Sci.& Technol. 2, 11 (2021). https://doi.org/10.1007/s42865-021-00041-w

550

Fountoulakis, I., Diémoz, H., Siani, A. M., di Sarra, A., Meloni, D., and Sferlazzo, D. M.: Variability and trends of the surface solar spectral ultraviolet irradiance in Italy: a possible influence of lower and upper stratospheric ozone trends, Atmos. Chem. Phys. Discuss. [preprint], https://doi.org/10.5194/acp-2021-616, in review, 2021.

555

Fioletov, V. E., Kimlin, M. G., Krotkov, N., McArthur, L. J. B., Kerr, J. B., Wardle, D. I., Herman, J. R., Meltzer, R., Mathews, T. W., and Kaurola, J. (2004), UV index climatology over the United States and Canada from ground-based and satellite estimates, J. Geophys. Res., 109, D22308, doi:10.1029/2004JD004820.

Fioletov, V., J. B. Kerr, A. Fergusson, The UV Index: Definition, Distribution and Factors Affecting It. Can. J. Public Health 101(4):I5-I9,2010.

562

Frederick, J. E., Koob, E. K., Alberts, A. D., and Weatherhead, E. C.: Empirical studies of tropospheric transmission in the ultraviolet: Broadband measurements, J. Appl. Meteorol., 32, 1883– 1892, 1993.

Reuder, J., and H. Schwander, Aerosol effects on UV radiation in nonurban regions, J. Geophys. Res., 104, 4065–4077, 1999

Giles, D. M. and Sinyuk, A. and Sorokin, M. G. and Schafer, J. S. and Smirnov, A. and Slutsker, I. and Eck, T. F. and Holben, B. N. and Lewis, J. R. and Campbell, J. R. and Welton, E. J. and Korkin, S. V. and Lyapustin, A. I., Advancements in the Aerosol Robotic Network (AERONET) Version~3 database -- automated near-real-time quality control algorithm with improved cloud screening for Sun photometer aerosol optical depth (AOD) measurements,Atmospheric Measurement Techniques, 12, 2019, 1, 169-209, https://www.atmos-meas-tech.net/12/169/2019/, DOI 10.5194/amt-12-169-2019.

J. Gröbner, J. Schreder, S. Kazadzis, A. F. Bais, M. Blumthaler, P. Gorts, R. Tax, T. Koskela, G. Seckmeyer, A. R. Webb, "A travelling reference spectroradiometer for routine quality assurance of spectral solar ultraviolet irradiance measurements", Applied Optics, 44 (25) 2005

He, S. and Carmichael, G. R.: Sensitivity of photolysis rates and ozone production in the troposphere to aerosol properties, J. Geophys. Res., 104, 26307–26324,https://doi.org/10.1029/1999JD900789, 1999

Holben, B.N., et al., 1998. AERONET—A federated instrument network and data archive for aerosol characterization. Remote Sens. Environ. 66, 1–16. https://doi.org/10.1016/S0034-4257(98)00031-5.

Ialongo, I., Buchard, V., Brogniez, C., Casale, G. R., and Siani, A.M.: Aerosol Single Scattering Albedo retrieval in the UV range:an application to OMI satellite validation, Atmos. Chem. Phys.,10, 331–340, https://doi.org/10.5194/acp-10-331-2010, 2010.

Iannarelli A.M, Di Bernardino, A., Casadio, S., Bassani, C., Cacciani, M., Campanelli , M., Casasanta, G., Cadau, E., Diémoz, H., Mevi, G., Siani, A. M., Cardaci, M., Dehn, A., Goryl, P.: The Boundary-layer Air Quality-analysis Using Network of INstruments (BAQUNIN) supersite for Atmospheric Research and Satellite Validation over Rome area, Bulletin of the American Meteorological Society, 2021, accepted.

International Ozone Service (IOS): International Ozone Service Inc., http://www.io3.ca/ (last access: 1 September 2018) September 2018

598 Kazadzis, S., Raptis, P., Kouremeti, N., Amiridis, V., Arola, A.,Gerasopoulos, E., and Schuster, G. L.:
599 Aerosol absorption retrieval at ultraviolet wavelengths in a complex environment, Atmos.Meas. Tech.,
600 9, 5997–6011, https://doi.org/10.5194/amt-9-5997-2016, 2016.

601

602 Kerr, J. B., and McElroy, C. T.: Evidence for large upward trends of ultraviolet-B radiation linked to
603 ozone depletion, Science, 262, 1032–1034, 1993.

604

605 Kinney, J. P., Long, C. S., and Geller ,A. C.: The Ultraviolet Index:A useful tool, Dermatol. Online J.,
606 6(1), 2, 1981.

607

608 Kirchstetter, T. W., Novakov, T., and Hobbs, P. V.: Evidence that the spectral dependence of light
609 absorption by aerosols is affected by organic carbon, J. Geophys. Res., 109, D21208,
610 https://doi.org/10.1029/2004JD004999, 2004.

611

612 Kudo, R., Diémoz, H., Estellés, V., Campanelli, M., Momoi, M., Marenco, F., Ryder, C. L., Ijima, O.,
613 Uchiyama, A., Nakashima, K., Yamazaki, A., Nagasawa, R., Ohkawara, N., and Ishida, H.: Optimal use
614 of the Prede POM sky radiometer for aerosol, water vapor, and ozone retrievals, Atmos. Meas. Tech.,
615 14, 3395–3426, https://doi.org/10.5194/amt-14-3395-2021, 2021.

616

617 Liu, C., Chung, C. E., Yin, Y., and Schnaiter, M.: The absorption Ångström exponent of black carbon:
618 from numerical aspects, Atmos. Chem. Phys., 18, 6259-6273, https://doi.org/10.5194/acp-18-6259-
619 2018.

620

621 Madronich, S., The Atmosphere and UV-B Radiation at Ground Level. In: Young A.R., Moan J., Björn
622 L.O., Nultsch W. (eds) Environmental UV Photobiology. Springer, Boston, MA, 1993

623

624 Madronich, S., 1993: UV radiation in the natural and perturbed atmosphere. Environmental Effects of
625 Ultraviolet Radiation, Lewis, Boca Raton,Florida. 17-69, Booth, C & Madronich, Sasha. Radiation
626 amplification factors: Improved formulation accounts for large increases in ultraviolet radiation
627 associated with Antarctic ozone depletion. Antarctic Research Series. 62. 39-42. 10.1029/AR062p0039,
628 1994.

629

Martins, J. V., Artaxo, P., Kaufman, Y. J., Castanho, A. D., and Remer, L. A.: Spectral absorption properties of aerosol particles from 350–2500 nm, Geophys. Res. Lett., 36, L13810, https://doi.org/10.1029/2009GL037435, 2009.

McKenzie, R. L., Matthews, W. A., and Johnston, P. V.: The relationship between erythemal UV and ozone, derived from spectral irradiance measurements, Geophys. Res. Lett., 18, 2269–2272, 1991.

Massabò D., Caponi, L., Bernardoni, V., Bove, M.C., Brotto, P., Calzolai, G., Cassola, F., Chiari, M., Fedi, M.E, Fermo, P., Giannoni, M., Lucarelli, F., Nava, S., Piazzalunga, A., Valli, G., Vecchi, R., Prati, P.: Multi-wavelength optical determination of black and brown carbon in atmospheric aerosols, Atmospheric Environment, Volume 108, 2015, Pages 1-12, ISSN 1352-2310, https://doi.org/10.1016/j.atmosenv.2015.02.058.

Meloni, D., A. di Sarra, G. Pace, and F. Monteleone, Optical properties of aerosols over the central Mediterranean. 2. Determination of single scattering albedo at two wavelengths for different aerosol types, *Atmos. Chem. Phys.*, **6**, 715–727, 2006.

Mok, J., Krotkov, N. A., Torres, O., Jethva, H., Li, Z., Kim, J., Koo, J.-H., Go, S., Irie, H., Labow, G., Eck, T. F., Holben, B. N., Herman, J., Loughman, R. P., Spinei, E., Lee, S. S., Khatri, P., and Campanelli, M.: Comparisons of spectral aerosol single scattering albedo in Seoul, South Korea, Atmos. Meas. Tech., 11, 2295-2311, https://doi.org/10.5194/amt-11-2295-2018, 2018.

Nakajima, T. and Tanaka, M.: Matrix formulation for the transfer of solar radiation in a plane-parallel scattering atmosphere. J. Quant. Spectrosc. Radiat. Transfer, 35, 13-2, 1986.

Nakajima, T., Campanelli, M., Che, H., Estellés, V., Irie, H., Kim, S.-W., Kim, J., Liu, D., Nishizawa, T., Pandithurai, G., Soni, V. K., Thana, B., Tugjsurn, N.-U., Aoki, K., Go, S., Hashimoto, M., Higurashi, A., Kazadzis, S., Khatri, P., Kouremeti, N., Kudo, R., Marenco, F., Momoi, M., Ningombam, S. S., Ryder, C. L., Uchiyama, A., and Yamazaki, A.: An overview of and issues with sky radiometer technology and SKYNET, Atmos. Meas. Tech., 13, 4195–4218, https://doi.org/10.5194/amt-13-4195-2020, 2020.

Panicker A. S., Pandithurai, G., Takamura, T. and Pinker, R. T.: Aerosol effects in the UV-B spectral region over Pune, an urban site in India Geophysical Research Letters, Vol. 36, L10802, doi:10.1029/2009GL037632, 2009.

Perrino C., Canepari, S., Catrambone, M., Dalla Torre, S., Rantica, E., Sargolini, T.: "Influence of natural events on the concentration and composition of atmospheric particulate matter" Atmospheric Environment, 43, 4766-4779, 2009.

Perrino C., Catrambone, M., Dalla Torre, S., Rantica, E., Sargolini, T., Canepari, S.: "Seasonal variations in the chemical composition of particulate matter: a case study in the Po Valley. Part I: macro-components and mass closure" Environ. Sci. Pollut. Res. 21, 3999-4009, 2014.

Perrino, C., Tofful, L. and Canepari, S. (2016), Chemical characterization of indoor and outdoor fine particulate matter in an occupied apartment in Rome, Italy. Indoor Air, 26: 558-570. doi:10.1111/ina.12235

Redondas, A., Carreño, V., León-Luis, S. F., Hernández-Cruz, B., López-Solano, J., Rodriguez-Franco, J. J., Vilaplana, J. M., Gröbner, J., Rimmer, J., Bais, A. F., Savastiouk, V., Moreta, J. R., Boulkelia, L., Jepsen, N., Wilson, K. M., Shirotov, V., and Karppinen, T.: EUBREWNET RBCC-E Huelva 2015 Ozone Brewer Intercomparison, Atmos. Chem. Phys., 18, 9441–9455, https://doi.org/10.5194/acp-18-9441-2018, 2018

Reuder, J., Schwander, H. Aerosol effects on UV radiation in nonurban regions First published: 01 February 1999 https://doi.org/10.1029/1998JD200072 Journal of Geophysical Research, Vol. 104, No. D4, Pages 4065-4077, February 27, 1999.

Schmalwieser, A.W., Gröbner, J., Blumthaler, M., Klotz, B., De Backer, H., Bolsée, D., Werner, R.,Tomsic, D., Metelka, L., Eriksen, P., Jepsen, N., Aun, M., Heikkilä, A., Duprat, T., Sandmann, H., Weiss, T., Bais, A., Toth, Z., Siani, A.M., Vaccaro, L., Diémoz, H., Grifoni, D., Zipoli, G., Lorenzetto, G., Petkov, B.H., Di Sarra, A.G., Massen, F., Yousif, C., Aculinin, A.A., Den Outer, P., Svendby, T., Dahlback, A., Johnsen, B., Biszczuk-Jakubowska, J., Krzyscin, J., Henriques, D., Chubarova, N., Kolarž, P., Mijatovic, Z., Groselj, D., Pribullova, A., Gonzales, J.R.M., Bilbao, J., Guerrero, J.M.V.,Serrano, A., Andersson, S., Vuilleumier, L., Webb, A., O'Hagan, J. UV Index monitoring in Europe (2017) Photochemical and Photobiological Sciences, 16 (9), 1349-1370

697

Siani, A.M., Modesti, S., Casale, G.R., Diemoz, H., Colosimo, A. Biologically effective surface UV climatology at Rome and Aosta, Italy (2013) AIP Conference Proceedings, 1531, 903-906, DOI: 10.1063/1.4804917

Siani, A.M., Frasca, F., Scarlatti, F., Religi, A., Diémoz, H., Casale, G. R., Pedone, M., Savastiouk, V.: Examination on total ozone column retrievals by Brewer spectrophotometry using different processing software, Atmos. Meas. Tech., 11, 5105–5123, 2018.

Slaper, H., Reinen, A. J. M., Blumthaler, M., Huber, M., and Kuik, F. Comparing ground-level spectrally resolved solar UV measurements using various instruments: a technique resolving effects of wavelength shift and slit width, Geophys. Res. Lett., 22, 2721–2724, 1995.

Vanicek, K. Differences between ground Dobson, Brewer and satellite TOMS-8, GOME-WFDOAS total ozone observations at Hradec Kralove, Czech. Atmos. Chem. Phys., 6, 5163–5171, 2006.

Venables, W. N. and Ripley, B. D.: Modern applied statistics with S-PLUS, Springer Science & Business Media, New York, 2013.